Spectroscopic observations of opacity in JET He discharges

OPEN ACCESS
IOP Publishing
Plasma Physics and Controlled Fusion
Plasma Phys. Control. Fusion **67** (2025) 105018 (12pp)
https://doi.org/10.1088/1361-6587/ae0eae

Spectroscopic observations of opacity in JET He discharges

K D Lawson[1,*], I H Coffey[1], M Groth[2], A G Meigs[1], S Menmuir[1], B Thomas[1] and JET Contributors[3]

[1] UKAEA(United Kingdom Atomic Energy Authority), Culham Campus, Abingdon, Oxfordshire OX14 3DB, United Kingdom
[2] Aalto University, Otakaari 1, Espoo 02150, Finland

E-mail: Kerry.Lawson@ukaea.uk

Received 14 April 2025, revised 14 July 2025
Accepted for publication 2 October 2025
Published 15 October 2025

Abstract

An understanding of the occurrence of opacity is important for modelling the power exhaust of magnetic confinement fusion plasmas. The absorption and reemission of radiation alters the magnitude and distribution of radiation within the divertor of the fusion machines, the plasma volume within the divertor controlling and limiting the power and particle fluxes to the plasma facing surfaces. High levels of opacity can also result in changes to the ionisation balance within the plasma. An analysis of a discrepancy between He II (He^{+}) line intensity measurements observed on the JET machine and the collisional-radiative models describing them has resulted in a better understanding of the behaviour of the radiation from He II. This has led to a simple technique for monitoring opacity within the He II ionisation stage. The technique has enabled three periods of He operations to be surveyed in order to determine the occurrence and severity of opacity in He discharges. A precise calculation of opacity is difficult, although estimates of escape factors and optical depths are possible for all pulses in which opacity is judged to be significant. These estimates do not fit the available line-of-sight opacity models and allow an alternative model that more closely matches the experimental results to be derived. The sensitivity of this model to its various components is discussed.

Keywords: He II opacity, Lyman series, JET, magnetic confinement fusion plasmas, VUV spectroscopic measurements

1. Introduction

The opacity of a plasma is its impenetrability to radiation, which can be due to either scattering or absorption by free or bound electrons. In laboratory plasmas it is only observed in regions of dense plasma in which there is a high population in the lower bound electronic level of the transition that led to the emission of the radiation. In magnetic confinement fusion plasmas, the energy level populations of fuel and impurity species are heavily biased towards the ground or metastable levels and, consequently, it is in the ground state transitions of the fuel with its high number density in which opacity is most likely to be seen. In hydrogen-like fuel ions, either a hydrogen isotope or helium, these transitions belong to the Lyman series.

The highest densities in magnetic confinement fusion plasmas occur in the divertor and an understanding of Lyman series opacity is crucial if the energy deposition on the divertor targets and walls is to be modelled accurately. Significant absorption and reemission of the Lyman radiation, which accounts

[3] See Maggi *et al* 2024 (https://doi.org/10.1088/1741-4326/ad3e16) for JET Contributors.
[*] Author to whom any correspondence should be addressed.

for ∼90% of the radiated power from the hydrogen-like fuel species, may alter the magnitude and distribution of the radiation within the divertor as well as affecting the ionisation balance. To illustrate these changes Wan *et al* (1995) have carried out detailed radiative transport modelling of a high-recycling, low T_e, H test case using the non-local thermodynamics equilibrium modelling code, CRETIN. This code is a subset of the GLF code (Scott and Mayle 1994) with additional neutral diffusion to ensure a self-consistent solution for this analysis. They find significant reabsorption of the H radiation as well as a change to the ionisation balance in their test case. Behringer and Fantz (2000) carried out collisional-radiative (CR) calculations for low T_e, H and D plasmas with He as an impurity, applicable to both technical and divertor plasmas. Molecular contributions and opacity are included. Opacity is treated through the use of escape factors (Behringer 1998) and their model is tested against measurements of Balmer alpha, beta and gamma line intensities, together with their ratios, emitted from an electron cyclotron resonance heated plasma. The effect of the He on the H and D Balmer ratios is also investigated.

There have been three earlier studies of opacity on JET, all dealing with D fuelled discharges. Lachin (1998) and Lovegrove *et al* (1995) present a detailed theoretical and experimental study in which the ratio of D Lyman beta and Balmer alpha line intensities is followed in four high density detached plasma pulses. A measured drop of ∼50% in the Lyman beta line intensity due to opacity along the line-of-sight of a VUV spectrometer is found to be somewhat larger than the calculated theoretical drop of up to 36%. Although the absorption of the Lyman alpha will be more severe, the analysis did not suggest a significant effect on the ionisation or power balance of the discharge. The Lyman alpha line had an optical thickness of ∼1, whereas an optical thickness closer to 6 is required for such changes. Nevertheless, the study highlighted the limitations of the divertor plasma modelling emphasising the need for the divertor transport simulation codes to include radiation transport.

A first attempt at including opacity corrections self-consistently in EDGE2D/NIMBUS simulations of high density JET L-mode discharges has been made by Maggi *et al* (1999). This followed observations that ratios of Lyman beta and Balmer alpha emission profiles again showed evidence of opacity in the inner divertor at high densities with a decrease in this ratio of ∼30%.

More recently Lomanowski *et al* (2020) has addressed opacity through a novel approach that considers the particle balance within the JET divertor.

A concurrent study applying SOLPS-ITER/EIRENE simulations to JET-ILW, D, L-mode discharges in which a radiation transport model has been restored to the EIRENE Monte-Carlo neutral transport code is being carried out by Chandra *et al* (2024). The photon transport model was initially developed by Reiter *et al* (2002) and Wiesen *et al* (2003) with full details being given by Wiesen (2005). The study is investigating the contribution of Lyman beta opacity to the Balmer alpha emission in low-recycling, high-recycling and detached discharges. Although low-recycling discharges are found to be optically thin, the Lyman alpha and beta emission is predicted to be reduced by at least a factor of 2 in some regions of the high-recycling and detached discharges.

An extensive review by Pshenov *et al* (2023) of both experimental and theoretical studies of divertor opacity in hydrogenic plasmas also demonstrates the importance of including photon transport both in transport simulations and in the interpretation of spectroscopic measurements of divertor emission. Opacity is found to have a strong impact on divertor plasma parameters increasing the local densities and reducing temperatures as well as affecting the atomic energy level populations; this leads to significant changes in the ionisation balance within the divertor plasma.

The present analysis follows on from a study of hydrogen-like He, in which a discrepancy was investigated between measurements on the JET tokamak and the CR models used to describe the Lyman line intensities (Lawson *et al* 2019, 2024). One possibility was that the discrepancy was due to opacity occurring routinely throughout all He-fuelled discharges. Although this was not confirmed, it did provide a good understanding of the Lyman series line emission and suggested a simple and novel method for monitoring opacity in He discharges. Using this method a survey of three He campaigns run on the JET tokamak has allowed discharges in which opacity has been observed to be catalogued, in order to inform the extent to which opacity affects JET discharges.

Information about the spectrometers used in making the measurements being used and further details of the experiments are given by Lawson *et al* (2024) and will not be repeated here. The next section gives the pertinent results of the He II analysis that has led to the method of monitoring opacity in He discharges. Its application to the He campaigns is given in section 3 and the derivation of a line-of-sight opacity model based on the experimental results is included in this section. The conclusions are presented in section 4.

2. Monitoring opacity in He discharges

Although similar discrepancies between the JET measurements and CR models were observed in both D I and He II Lyman line intensities, there are advantages in studying He discharges in the first instance. They have fewer impurities, meaning that the spectra are less complicated and so the analysis is more reliable. Further, there are no molecular contributions to the populations of excited energy levels in He ions as occurs in the D atoms. Not only does the He study inform that of D, the behaviour and description of He is important in its own right. He is a product of DT fusion reactions as well as a possible discharge fuel used to avoid machine activation. Therefore, to model fully a burning plasma, it is necessary that the behaviour of He is understood. Figure 1 shows an example

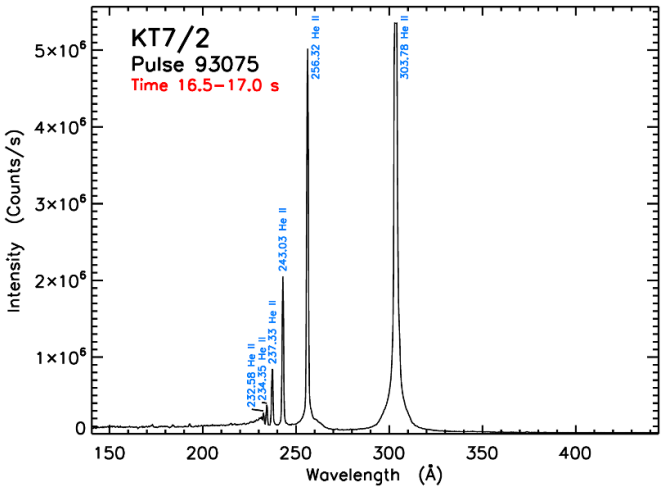

Figure 1. The spectrum of pulse 93 075 averaged between 16.5–17.0 s recorded with KT7/2, chosen to display the He Lyman series. Although saturated the Lyman α line can be reliably reconstructed.

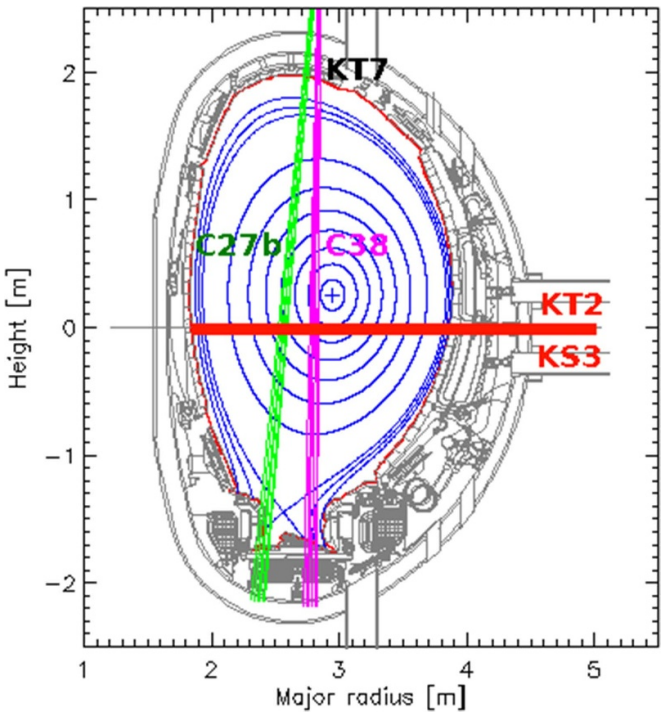

Figure 2. Lines-of-sight of the KS3, KT2 and KT7 spectrometers used during the JET C27b and C38 campaigns, together with the magnetic configuration at 17 s in pulse 93 048.

of a VUV spectrum of a He discharge in which the Lyman series is seen (Lawson *et al* 2024). This is recorded by the KT7 survey spectrometer which views the JET divertor along a vertical line-of-sight (figure 2) and is averaged over a time 16.5–17.0 s in JET pulse 93 075. In this spectrum all the lines are identified with He.

The failure of the CR models to describe adequately the JET He II observations means that there is uncertainty regarding the electron temperature of the plasma region emitting the He II radiation. Arnaud and Rothenflug (1985) give a temperature of maximum He II ion abundance of ∼4–5 eV. In non-coronal equilibrium the distribution of charge states can be described by the product of electron density and residence time, with Huber *et al* (2021) finding a somewhat higher temperature of ∼6–7 eV for a typical value of 0.3×10^{17} m^{-3}.s for this product. These values would be consistent with estimates from the CR modelling. It is expected that there will be a range of densities in the discharges being studied, typically 10^{19}–10^{20} m^{-3}.

The extensive survey of the He II line intensities led to an unexpected result in that the Lyman line intensities are found to have constant ratios and this applies whether the observation is made along a vertical or horizontal line-of-sight. Furthermore, the value of the ratios does not depend on the line-of-sight, within errors being the same for both vertical lines-of-sight from the top of the machine into the divertor and a horizontal line-of-sight viewing the main chamber, the lines-of-sight being shown in figure 2 (Lawson *et al* 2024). This reproducibility is illustrated in figure 3 for the horizontal line-of-sight. Each point represents the ratio of the Lyman alpha to beta line intensities recorded by the KT2 spectrometer, the intensities being averaged over half second intervals. The figure includes data throughout all the pulses in the JET-ILW C38 He restart (figure 3(a)). Information regarding the experiments is given by Lawson *et al.* As explained in this reference the range of plasma parameters is limited during the period of the restart operations, in particular there being no additional heating. Nevertheless, the only selection of the data has been to set a minimum Lyman alpha intensity in order to minimise noise and a similar result is found during the C38 He experiment when additional heating was applied to the plasma (figure 3(b)). A few excursions of the Lyman alpha to beta ratio to higher values are observed, but the vast majority of points lie in a narrow band.

The near-constant ratios are also observed when viewing the divertor. In this case the higher spectral resolution of the short wavelength VUV survey spectrometer (KT7/2) allows a number of Lyman lines to be observed and up to five line intensity ratios to be measured. Figure 4 illustrates time histories of the lowest 6 Lyman series members in pulse 93 048, up to and including the $n = 1-7$, Lyman zeta line. This is a 2.2 T, 1.8 MA discharge run during the JET-ILW, C38 restart. It is necessary to carry out line fitting to obtain the intensity of the blended Lyman zeta line. This was only successful for some of the time slices, resulting in a series of points being shown. As with the KT2 data with its horizontal view the line intensity ratios are observed to be near constant throughout this pulse, with values of the ratios given in the figure.

Figure 3 shows that a few pulses have points which lie above the general trend, this mainly being observed when the He intensities are high. Figure 5 shows the time histories of the Lyman series lines observed with KT7/2 for one of these pulses, an Ohmic discharge number 93 056, run during the He

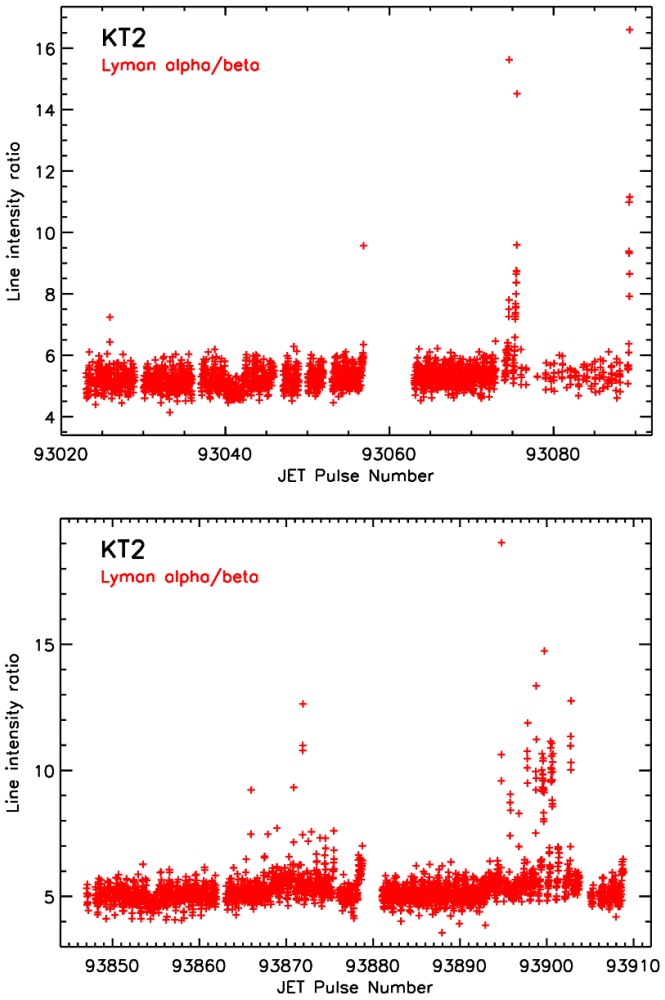

Figure 3. (a). The Lyman α to β ratio recorded with KT2 during the JET-ILW C38 He restart, with a minimum Lyman α intensity of 8.6×10^{18} ph $s^{-1} \cdot m^{-2} \cdot sr^{-1}$. (b). The Lyman α to β ratio recorded with KT2 during the JET-ILW C38 He experiment, with a minimum Lyman α intensity of 8.6×10^{18} ph $s^{-1} \cdot m^{-2} \cdot sr^{-1}$.

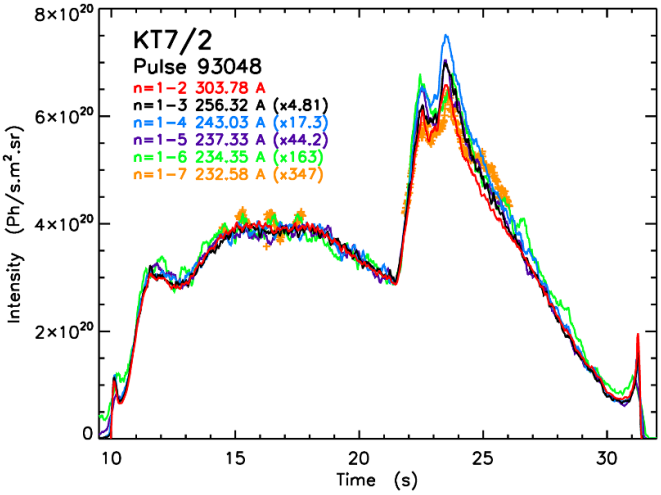

Figure 4. Lyman series line intensities for pulse 93 048 recorded with KT7/2 during the JET-ILW C38 He restart.

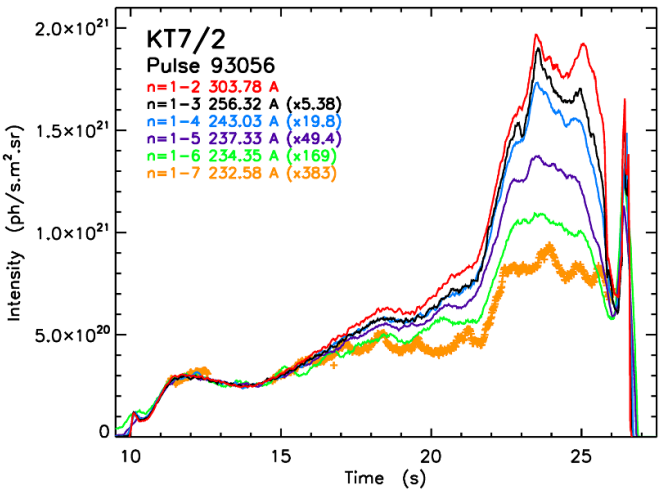

Figure 5. The Lyman series line intensities for pulse 93 056 recorded with KT7/2 during the JET-ILW C38 He restart.

restart, in which the line intensity ratios are seen to increase during the pulse. This pulse is similar to pulse 93 048 except that the density continues to rise, whereas in pulse 93 048 the density plateaus at 15.5 s. As in figure 4 the Lyman zeta line intensity was obtained by line fitting and hence is shown as a series of points.

What is less usual and seen only at the highest He line intensities (the Lyman alpha line $\sim 10^{21}$ ph $s^{-1} \cdot m^{-2} \cdot sr^{-1}$ and above) is for the line intensity ratios to decrease during a pulse. If the largest decrease is observed for the Lyman alpha line intensity, the line most affected by opacity, with smaller decreases for the Lyman beta line and higher series members, this is taken to be an indication that absorption is taking place along the line-of-sight of the observing instrument. Although absorption is followed by a rapid spontaneous decay, the photon is reemitted in an arbitrary direction and the narrow field of view of the VUV spectrometers means that there is a low probability ($\sim$1 in 10^{-10}) of the photon being emitted with a direction within the acceptance angle of the spectrometer enabling it to pass through the narrow entrance slit (2.5 mm $\times$ 25 μm) of the instrument which is $\sim$6.8 m from the divertor. The limited size of the divertor plasma ensures that the spectrometer's field of view is not filled by photons emitted from excited atoms moving from other parts of the divertor, although these are expected to make some contribution to the observed intensity. Allowance for this contribution is made in the line-of-sight opacity models used to predict the reduction in the Lyman series line intensities. It follows that opacity can be monitored simply by following the Lyman series line intensities and checking to see when the Lyman alpha to beta ratio and to a lesser extent the Lyman beta to gamma ratio decrease, with the proviso that this will only be an indication of opacity when the He intensities are high. The subsequent analysis relies on this method for indicating the occurrence of opacity.

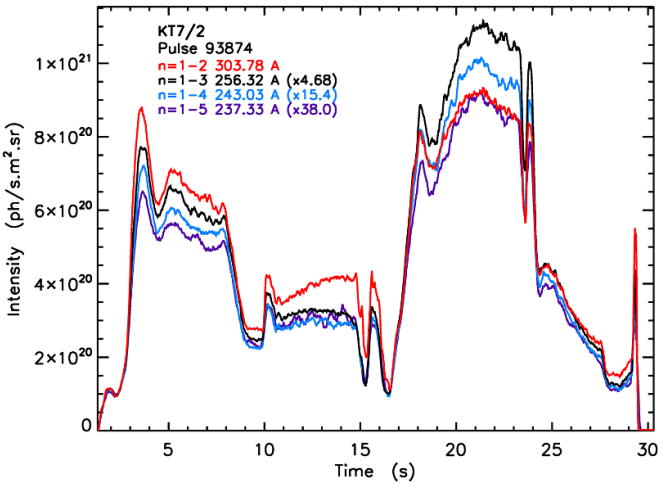

Figure 6. Lyman series line intensities for pulse 93 874 recorded with KT7/2 during the JET-ILW C38 He experiment.

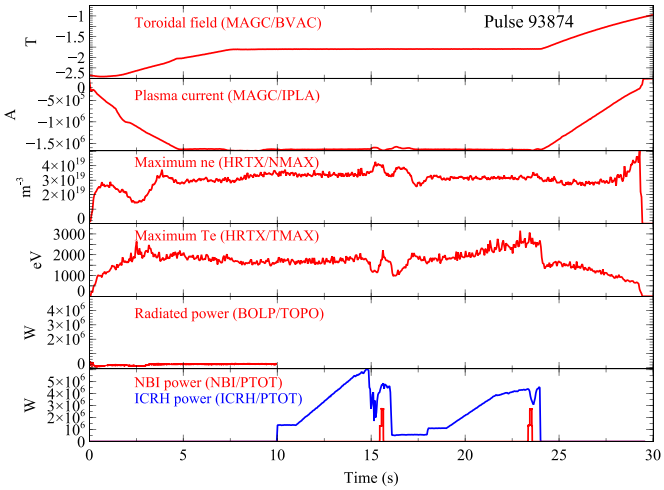

Figure 7. Plasma parameters for pulse 93874.

3. Application to JET He campaigns

3.1. Monitoring opacity

In monitoring opacity a search has been made for the Lyman alpha to beta ratio decreasing at high He intensities, this being used as an indication that opacity is having a significant effect on the observed line intensities. This behaviour is seen, for example, in the 1.8 T, 1.6 MA discharge, pulse 93 874, for which the time histories of the line intensities are shown in figure 6. It was run during the C38 He experiment as part of an investigation into the L- to H-mode transition in He plasmas (Solano *et al* 2021). The discharge parameters are shown in figure 7, there being ion cyclotron resonance heating (ICRH) with neutral beam injection (NBI) blips used for diagnostic purposes. In the first heating phase the Lyman alpha line follows the expected high intensity behaviour as is seen earlier in the pulse rising above the scaled line intensities of the other observed Lyman series lines. However, in the second heating phase after the plasma configuration switches from the outer strike point falling on tile 5 (V5 configuration) to a corner configuration, the intensities are significantly higher. The Lyman alpha line intensity drops below its expected trajectory, indicating that opacity is playing a role. Only the Lyman series lines up to the Lyman delta line could be reliably measured in this pulse. The Lyman epsilon line at 234.35 Å is blended with the strong 234.15 Å, Ni XXVI line, this blending also affecting the line fitting procedure used to determine the intensity of the Lyman zeta line at 232.58 Å. Even the Lyman delta line observed during the first heating phase is at the limit of what can be reliably measured for the higher series members.

3.2. Survey of pulses showing optical depth

Using the Lyman alpha to beta ratio as a monitor, a check has been made of the occurrence of opacity in He-fuelled discharges for three periods of operations, one in campaign C27b and the He restart and experiment in C38. It is noted that there is no evidence of opacity affecting the KT2 observations made along a horizontal line-of-sight viewing the main chamber plasma. Table 1 provides the results of the survey for the divertor view recorded with the KT7/2 spectrometer, with the opacity being classified as significant or marginal. Significant opacity corresponds to a period of more than 2 s of the discharge being affected. All of the pulses in which opacity is observed have intense He emission, although this is not the only criterion required for opacity to be significant. During the C27b campaign KT7/2 viewed the inner vertical target plates of the divertor, while in the C38 campaign the view was towards an outer section of the horizontal divertor tile 5 (figure 2). The plasma densities in the inner divertor tend to be higher and consequently opacity is expected to be more severe along the inner divertor line-of-sight used during C27b. It can be seen that opacity does affect a significant proportion of pulses in both C27b and the C38 He experiment, additional heating being used in both.

3.3. Opacity

The probability of an emitted photon traversing a distance D through an absorbing plasma is given by Holstein (1947) as the transmission,

$$T(D) = \int_{-\infty}^{\infty} \phi(\nu)\, e^{-k(\nu)D}\, \mathrm{d}\nu,$$

where $k(\nu)$ is the absorption coefficient and $\phi(\nu)$ is the emission profile of the spectral line, which is normalised such that,

$$\int_{-\infty}^{\infty} \phi(\nu) = 1.$$

Table 1. Frequency of pulses affected by opacity.

Campaign	JET-C C27b He campaign	JET-ILW C38 He restart	JET-ILW C38 He experiment
Dates	August–September 2009	October 2018	June 2019
Pulses	78 907–79 243	93 023–93 089	93 847–93 908
Significant opacity	12	0	9
Marginal opacity	16	1	9
Total no. of pulses	244	54	59
Percentage of pulses with significant opacity	4.9	—	15.3

In general,

$$\int_{-\infty}^{\infty} k(\nu)\,\mathrm{d}\nu = \frac{\lambda_0^2 g_2 n A}{8\pi g_1},$$

where λ_0 is the wavelength, g_1 and g_2 are the statistical weights of the lower and upper levels, respectively, and A the spontaneous transition probability or A-value. n is the ion density. In the plasmas being investigated, the dominant mechanism determining the line profile will be Doppler broadening resulting from the motion of the ions. Assuming a Maxwellian velocity distribution,

$$k(\nu) = k_0 \exp\left[-\left(\frac{\nu-\nu_0}{\nu_0}\right)^2\left(\frac{c}{u}\right)^2\right],$$

where the velocity

$$u = \left(\frac{2kT_i}{m}\right)^{1/2}$$

and

$$k_0 = \frac{\lambda_0^3\, n\, g_2\, A}{8\pi^{3/2} g_1\, u}. \qquad (1)$$

Applying equation (1) to a 6 eV, He II plasma with ion densities, $n+$, of 10^{19} and 10^{20} m^{-3} it can be seen in figure 8 that the absorption of Lyman radiation can be significant. This is particularly so for the Lyman alpha radiation, although all series members are affected to a lesser or greater extent.

3.4. The escape factor

The most convenient treatment of opacity in the present analysis uses the escape factor methodology. The escape factor is the effective reduction in the spontaneous transition probability or A-value as a result of the emission being absorbed. It has been calculated by a number of authors, their calculations being summarised and compared by Irons (1979). He considers two geometries, an infinite plane-parallel slab and an infinite cylinder. The models discussed include those with Gaussian, Lorentzian and Holtsmarkian spectral line profiles. In the present case, Doppler broadening determines the line profile and hence the analysis for the infinite plane-parallel slab with the Gaussian line profile is used. The escape factor for this case plotted against the product of the absorption coefficient and distance a photon travels, k_0D, is illustrated in figure 9, which is based on figure 1 of Irons. The upper limit shown in this diagram corresponds to the case where there is uniform excitation and hence emission throughout the plasma volume. The lower limit corresponds to the other extreme in which the emission results from a narrow region that, in the limiting case, corresponds to a delta function. The analysis assumes that the spectral line profiles of the emitting and absorbing lines are identical.

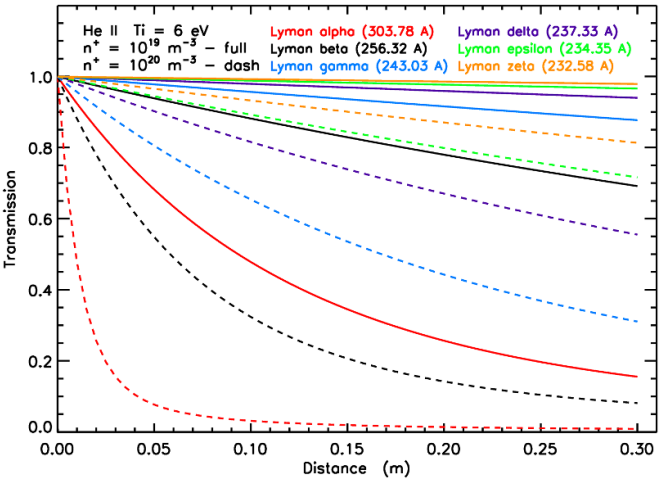

Figure 8. Transmission of an emitted Lyman series photon through a He II plasma with T_i of 6 eV and n^+ of 10^{19} and 10^{20} m^{-3}.

3.5. Estimation of the escape factor and optical depth

The most satisfactory method of measuring the escape factor involves comparisons with lines from higher spectral series. This would allow the reduction in the Lyman intensities to be measured directly. However, higher series members that would enable this for He II are not observed by the spectroscopic diagnostics available on JET. An alternative method would involve calculating k_0D for which there are large uncertainties not only in estimating the distance traversed by a Lyman photon, but also in the He II ion density and temperature profiles needed to determine the absorption coefficient k_0.

Consequently, a method is used which makes use of the extensive survey of the Lyman line intensities in the three periods of operation being studied, which has led to a better understanding of the behaviour of the line intensity time histories. As shown in figure 3 the Lyman line intensity ratios

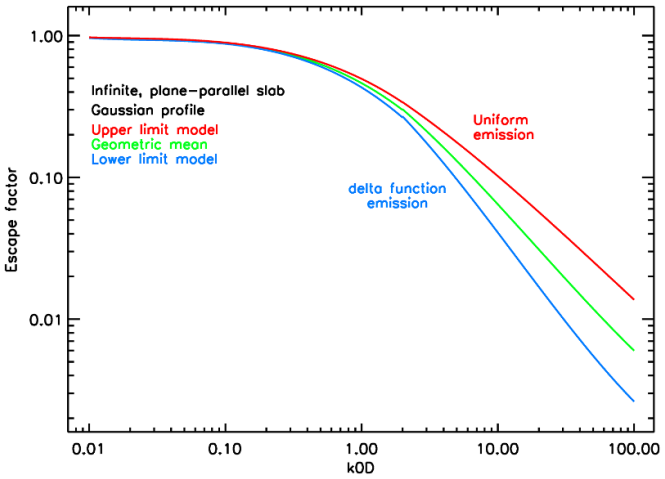

Figure 9. The escape factor calculated for an infinite plane parallel slab for a spectral line with a Gaussian profile. The upper limit corresponds to the case with uniform emission throughout the absorbing plasma, the lower limit to a delta function emission (after figure 1 of Irons 1979).

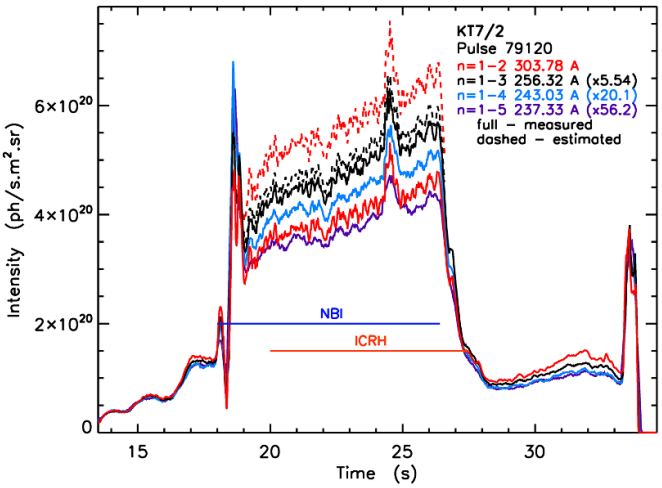

Figure 10. Lyman series line intensities for pulse 79 120 recorded with KT7/2 during the JET-C C27 He campaign, showing the expected trajectories of the Lyman alpha and beta lines.

are near-constant or, at high He intensities, increase as is illustrated in figures 5 and 6 and subsequent figures. In determining the escape factors, the constant ratios for the pulse being considered is found during the low intensity phase. Although the ratios fall in the ranges illustrated in figure 3 and by Lawson *et al* (2024) small variations can lead to significant differences during the later high intensity phases of the pulse. Hence it is essential to determine the precise ratios for each pulse investigated.

In all pulses in which opacity is found to be significant the He intensities are high enough for increases in the ratios to be expected. A typical increase of ∼15% is supposed between the time histories of consecutive Lyman lines in order to give estimated 'unabsorbed' line intensities. The escape factor is then the ratio of the observed line intensity to the 'unabsorbed' line intensity.

To see whether this procedure is useful it is necessary to consider the errors that might result particularly from the positioning of the 'unabsorbed' line intensity. Reducing its intensity by ∼15% will mean that unexpectedly there is no increase in the ratio, while increasing the intensities by ∼15% results in a behaviour in which the trajectories are significantly higher than is typically found. It should therefore be possible to position the 'unabsorbed' line trajectory to within ∼±15%. In cases in which the opacity is large the positioning of the 'unabsorbed' time histories has only a small impact on the derived escape factors, these depending more strongly on the shortfall in the observed time history. The escape factor, T, is related to the frequency averaged optical depth, $\tau_{\rm av}$, by the equation,

$$T = \frac{1 - \exp\left(-\tau_{\rm av}\right)}{\tau_{\rm av}}$$

with the optical depth at line centre, τ_0, given by $\sqrt{\pi}\,\tau_{\rm av}$ for Gaussian spectral line profiles (Tallents 2018, 2019). This allows estimates of the optical depth to be derived from the escape factors.

The procedure described above is illustrated for several pulses in figures 10–13. Pulse 79120 is a 1.8 T, 1.7 MA discharge run during an L- to H-mode transition and confinement experiment in JET-C C27b. An initial 13.2 MW of He NBI trips after 0.7 s resulting in a steady 6.8 MW throughout the rest of the NBI heating phase. The additional heating also includes 2 MW of ICRH. The increase of the Lyman gamma line intensity above that of the Lyman delta line intensity is repeated in order to position the Lyman alpha and beta line trajectories as shown in figure 10. As explained above, it can be seen that a ∼±15% error in the placing of the Lyman alpha trajectory would mean either that unexpectedly there is no increase in the Lyman alpha to beta ratio at all or that the Lyman alpha trajectory would reach over $\sim 7.5 \times 10^{20}$ ph $\mathrm{s}^{-1} \cdot \mathrm{m}^{-2} \cdot \mathrm{sr}^{-1}$ at 26 s, both of which would deviate from the observed typical behaviour. The positioning of the 'unabsorbed' time histories for the Lyman alpha and beta lines then allows the escape factors for these lines to be estimated.

Pulse 79 143 is from the same experiment, but with a lower field and current of 1.1 T and 1.0 MA and with only NBI (10 MW) additional heating. Figure 11(a) shows the observed Lyman alpha to delta line intensities, with predicted trajectories without absorption shown in figure 11(b). Pulse 79 180 is from a different experiment in which magnetic perturbations are used to investigate the control of ELMs. The discharge has a toroidal field and current of 1.9 T and 1.8 MA with both He NBI (13.9 MW from 13.0–19.45 s) and ICRH (2.2 MW from 16–19.3 s). In this pulse the Lyman alpha, beta and gamma lines are affected by opacity (figure 12). Finally, the Lyman series line intensities, together with the predicted, unabsorbed Lyman alpha and beta trajectories, are illustrated in figure 13 for the JET-ILW pulse 93 879, part of an L- to H-mode transition investigation. As in pulse 93 874 (figure 6) there are two periods of ICRH with D NBI blips, the field, current and heating waveforms (figure 7) being similar for both pulses. The ICRH reaches 6.5 and 6.1 MW, respectively,

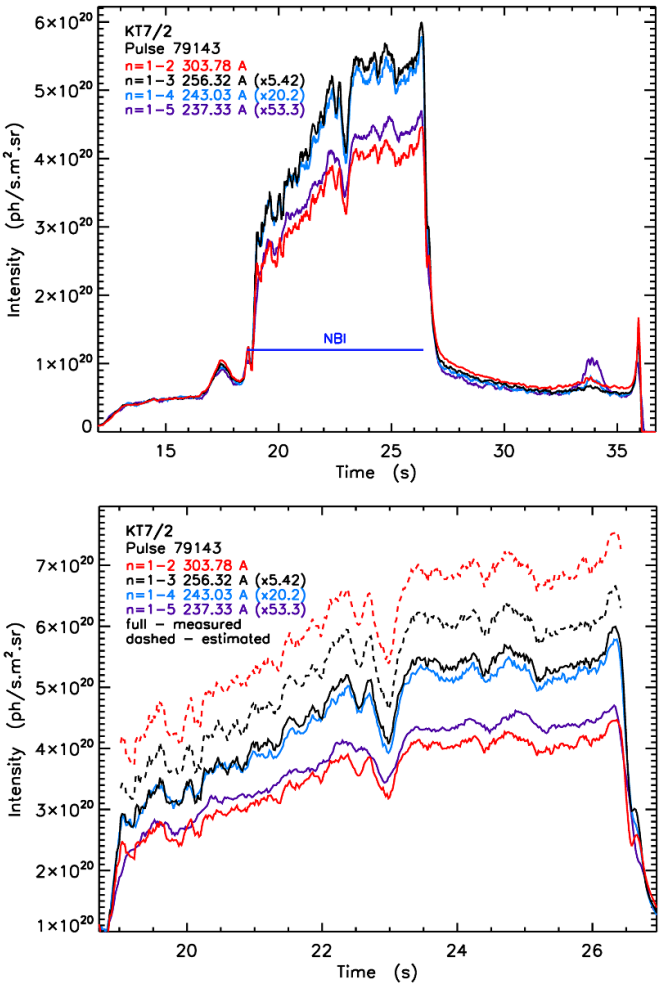

Figure 11. (a). Measured Lyman series line intensities for pulse 79 143 recorded with KT7/2 during the JET-C C27 He campaign. (b). Lyman series line intensities for pulse 79 143 recorded with KT7/2 during the JET-C C27 He campaign, showing the expected trajectories of the Lyman alpha and beta lines.

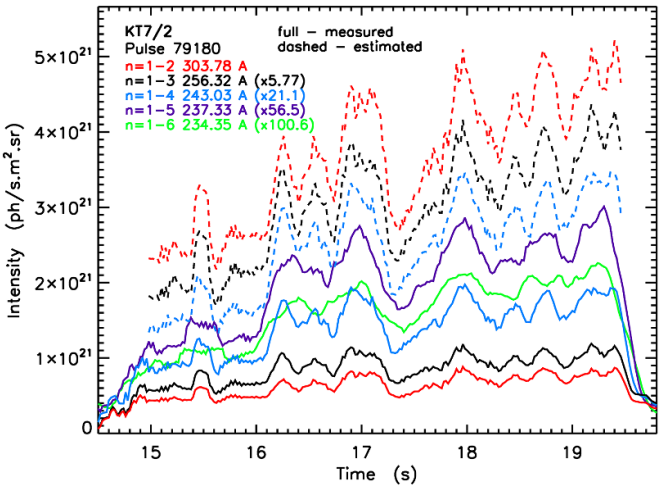

Figure 12. Lyman series line intensities for pulse 79 180 recorded with KT7/2 during the JET-C C27 He campaign, showing the expected trajectories of the Lyman alpha, beta and gamma lines.

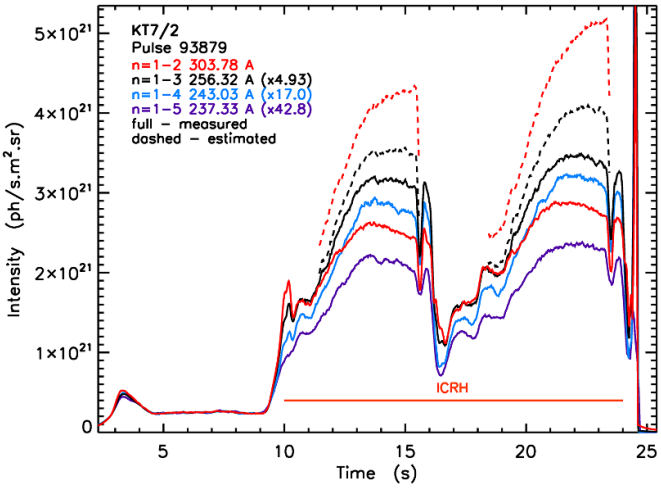

Figure 13. Lyman series line intensities for pulse 93 879 recorded with KT7/2 during the JET-ILW C38 He experiment, showing the expected trajectories of the Lyman alpha and beta lines.

in the 2 heating phases in the later discharge. However, in pulse 93 879 significant opacity is seen during both ICRH periods.

Table 2 lists the time intervals over which opacity is observed as well as estimates of the escape factors and optical depths for all pulses in which the opacity is judged to be significant. Since transport simulation codes used for He are generally not equipped to deal with photon transport, particular care should be taken if any of these pulses are used for transport modelling.

Although measurements of density in the JET divertor are not available, the divertor density closely correlates with the main chamber edge density. Figure 14 shows the dependence of opacity on the line integrated edge density for the JET-C pulses. It can be seen that those pulses in which the Lyman alpha opacity is estimated to be highest have the highest edge densities.

A comparison of the total ion flux reaching the outer divertor target plates is shown in figure 15 for pulses 93 874 and 93 879, the latter having the highest estimated opacity of the JET-ILW pulses. As mentioned above, these two pulses are similar, although an increased fuelling rate and higher ICRH power in pulse 93 879, particularly in the second period of ICRH (6.1 MW as opposed to 4.4 MW), leads to a consistently higher maximum electron density in pulse 93 879 of 5.0×10^{19} m^{-3} compared with 3.3×10^{19} m^{-3} in pulse 93 874 throughout the period of additional heating. It can be seen that there is evidence for the onset of detachment at 13.8 s and again at 22.0 s in pulse 93 879. It is noted that the lower intensities and ion fluxes in the earlier heating phase of pulse 93 874 correspond to the plasma having a V5 configuration, whereas a corner configuration is used throughout in pulse 93 879.

3.6. Line-of-sight opacity model

Comparisons between the Lyman escape factors listed in table 2 and the infinite plane-parallel slab model (figure 9)

Table 2. Estimates of escape factors and frequency averaged optical depths for pulses in which opacity is significant.

		Lyman escape factors			Lyman optical depth		
Pulse number	Time (s)	Alpha	Beta	Gamma	Alpha	Beta	Gamma
JET-C							
79 120	19.0–26.6	0.70	0.95	—	0.75	0.10	—
79 129	19.6–23.0	0.53–0.66	0.71–0.85	0.88–0.95	1.44–0.91	0.73–0.34	0.27–0.10
79 129	23.3–26.5	0.71	0.96	—	0.72	0.08	—
79 130	18.9–21.9	0.51–0.63	0.67–0.74	0.83–0.90	1.53–1.03	0.86–0.63	0.40–0.21
79 130	22.4–25.9	0.77–0.78	0.91–0.88	—	0.55–0.53	0.21–0.26	—
79 133	21.7–23.9	0.63–0.65	0.88–0.86	—	1.03–0.95	0.27–0.31	—
79 133	24.5–26.5	0.70–0.69	0.94–0.95	—	0.76–0.80	0.12–0.10	—
79 137	20.9–23.9	0.62	0.89–0.86	—	1.04	0.25–0.32	—
79 138	20.0–23.9	0.61–0.67	0.84–0.88	—	1.10–0.86	0.36–0.26	—
79 143	19.0–26.4	0.59	0.86–0.90	—	1.18–1.16	0.32–0.21	—
79 162	13.5–15.6	0.71–0.54	0.97–0.95	—	0.72–1.42	0.06–0.10	—
79 162	16.8–17.6	0.22–0.33	0.33–0.50	0.51–0.63	4.45–2.82	2.82–1.59	1.53–1.03
79 164	9.82–13.0	0.73–0.74	0.96	—	0.67–0.63	0.09	—
79 164	13.3–14.3	0.79–0.50	1.0–0.94	—	0.50–1.59	0.00–0.14	—
79 164	14.9–15.0	0.30–0.21	0.47–0.36	0.77–0.61	3.18–4.71	1.77–2.53	0.55–1.10
79 180	15.0–19.5	0.19–0.17	0.32–0.27	0.61–0.56	5.27–5.99	2.99–3.60	1.10–1.32
79 181	15.6–21.0	0.31–0.41	0.42–0.55	0.69–0.80	3.05–2.17	2.11–1.36	0.80–0.47
79 203	15.5–20.5	0.51–0.64	0.63–0.85	0.85–1.00	1.53–0.98	1.03–0.34	0.34–0.00
JET-ILW							
93 870	9.20–14.9	1.00–0.77	—	—	0.00–0.55	—	—
93 870	18.3–23.3	1.00–0.61	1.0–0.84	—	0.00–1.10	0.00–0.36	—
93 872	19.0–22.5	0.93–0.82	0.97–0.95	—	0.16–0.41	0.07–0.10	—
93 874	19.0–23.4	0.84–0.73	—	—	0.36–0.68	—	—
93 878	13.4–15.5	0.91–0.78	—	—	0.19–0.52	—	—
93 878	18.3–23.4	1.00–0.63	1.00–0.84	—	0.00–1.00	0.00–0.36	—
93 879	11.4–15.6	0.78–0.56	0.94–0.88	—	0.52–1.32	0.12–0.27	—
93 879	18.4–23.4	0.83–0.52	0.95–0.83	—	0.38–1.50	0.10–0.40	—
93 897	10.0–13.0	0.82–0.78	1.00–0.93	—	0.41–0.52	0.00–0.16	—
93 898	10.1–13.0	0.87–0.81	—	—	0.29–0.43	—	—
93 903	10.3–12.9	0.87	—	—	0.29	—	—
93 908	20.4–22.3	0.80–0.86	0.92–0.96	—	0.47–0.32	0.18–0.08	—
93 908	22.4–23.6	0.76–0.74	0.89–0.89	—	0.58–0.65	0.23–0.25	—
93 908	23.6–24.9	0.74–0.81	0.89–0.90	—	0.65–0.43	0.25–0.21	—

show that these data are not a good fit to the model. This is thought in part due to the finite size of the divertor plasma. Nevertheless, an alternative model that better fits the data can be derived from the escape factors determined from the present observations. It is assumed that the same dependence on k_0D applies to both the Lyman alpha and beta lines and uses the fixed relationships between the absorption coefficients for the Lyman lines. From equation (1) it can be seen that the ratios are independent of density and temperature and they are given in table 3. Hence, the same curve for the Lyman alpha and beta escape factor dependence on k_0D is used with the value of k_0D for the Lyman beta line reduced from that for Lyman alpha by a factor 6.24. Those data presented in table 2 with a Lyman gamma escape factor <1 together with data from another C27b discharge, pulse 79 130 at 22.38 s, are fitted to a 3rd order polynomial. This is achieved by minimising the squared differences between the measured and modelled escape factors, the latter being determined from the polynomial fit. The value of k_0D for each Lyman alpha data point together with the four coefficients of the polynomial are allowed to vary in the minimisation. This selection of data gives a wide range of measured escape factors, the data point from pulse 79 130 extending the range to an escape factor close to 1. It nevertheless only includes C27b pulses for which the line-of-sight and therefore plasma geometry are the same.

The empirical model derived in this way is shown in figure 16, in which it is compared with the infinite plane parallel slab model with uniform emission throughout the plasma volume (figure 9, after Irons 1979); it is seen to have a slower fall-off with increasing k_0D. Clearly, the accuracy of the estimates of the escape factors will be a limiting factor in this model. For the Lyman alpha and beta lines, this is expected to be $\sim\pm15\%$. Another consideration is the plasma geometry. Data from the C38 He experiment, for which the line-of-sight was towards the outer divertor, will give some indication of the sensitivity of the model to the geometry and are included in

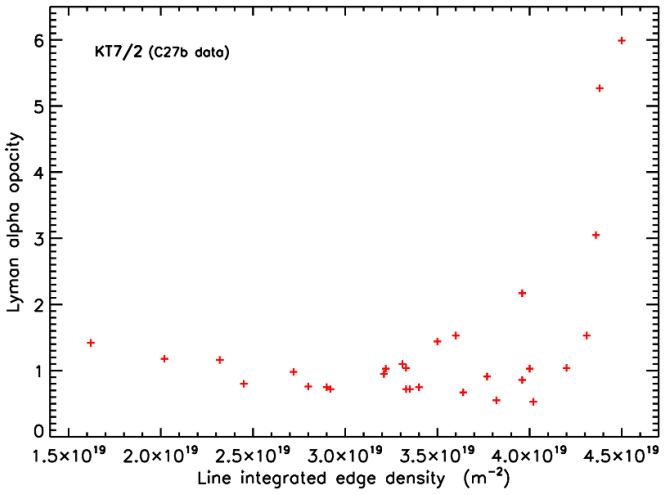

Figure 14. The dependence of the estimated Lyman alpha opacities on the main chamber line integrated edge density.

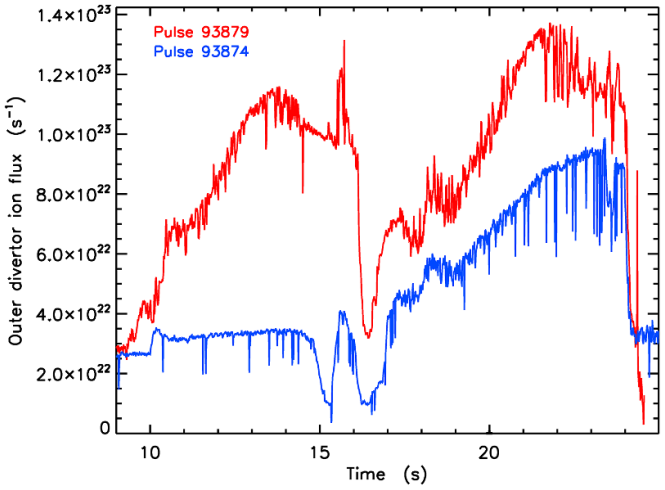

Figure 15. The total outer divertor ion flux in pulses 93 874 and 93 879.

figure 17. There is no indication from these data that the model is particularly sensitive to the different geometries resulting from the two lines-of-sight, although the range of k_0D for the C38 measurements is limited. The assumption that the escape factors for the Lyman alpha and beta lines are described by the same model is dependent on geometric factors relating to the distribution of emission and absorption throughout the observed plasma volume, as well as on the spectral line profiles for the emission and absorption. That these factors may have a significant influence on the derived model is suggested by plotting the available data for the Lyman gamma line with the values of k_0D reduced by a factor 17.95. The trend of these points, shown in figure 18, lies above that for the Lyman alpha-beta model. Even allowing for a somewhat poorer accuracy of $\sim\pm20\%$ for the Lyman gamma points the difference at the highest values of k_0D has reached the limit of what can be accommodated within errors. Calculating the length of the

Table 3. Ratios of the absorption coefficients for the Lyman lines.

Lyman lines	Alpha/beta	Alpha/gamma	Alpha/delta
Ratio	6.236	17.95	38.22

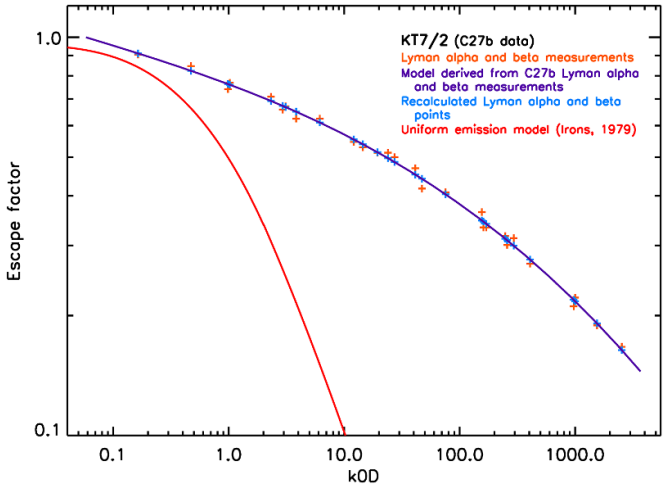

Figure 16. Comparison of the escape factor model derived from the C27b Lyman alpha and beta measurements and the uniform emission model of Irons (1979).

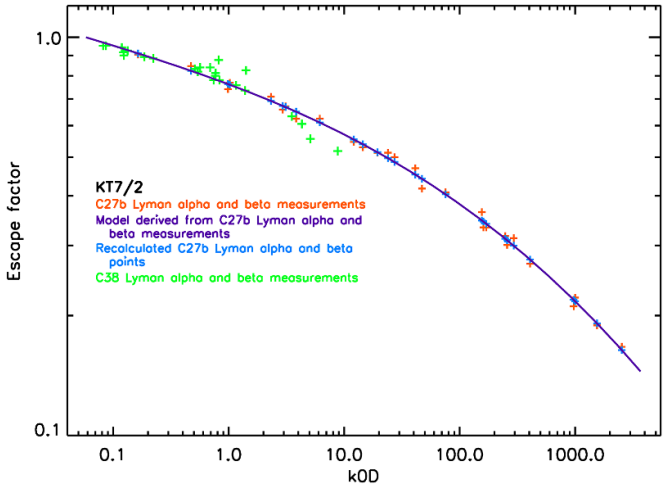

Figure 17. The escape factor model derived from the C27b Lyman alpha and beta measurements together with data from the C38 He experiment.

emission/absorption plasma region, D, shows that the model is compatible with typical divertor parameters, although this length depends strongly on the ion density and, consequently, this is not a particularly stringent test. The optical depths listed in table 2 are of a magnitude that would be expected to lead to a redistribution of radiation within the divertor. However, apart from pulse 79 180 they are less than $\sim$6 at which changes in the ionisation balance become important (Lachin 1998).

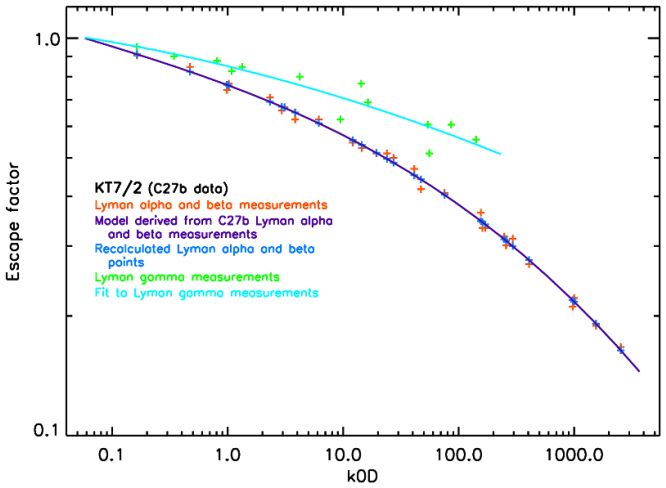

Figure 18. The escape factor model derived from the C27b Lyman alpha and beta measurements together with the C27b Lyman gamma measurements.

4. Conclusions

A simple and novel technique for monitoring opacity has been used to survey three He campaigns run on the JET tokamak. It derives from a better understanding of the behaviour of the hydrogen-like He emission following from an analysis to understand a discrepancy between the He II line intensities and the CR models used to describe them (Lawson *et al* 2024). The technique is based on the observation that the line intensity ratios of the He II Lyman series are near-constant or, at high He line intensities, the Lyman alpha to beta, beta to gamma, etc. ratios increase. However, at the highest He line intensities (the Lyman alpha line $\sim 10^{21}$ ph $s^{-1} \cdot m^{-2} \cdot sr^{-1}$ and above) the Lyman alpha to beta and to a lesser extent the Lyman beta to gamma ratios can also be seen to decrease and this is taken to be an indication of the Lyman line intensities being reduced through absorption, the Lyman alpha line being most affected by opacity.

The survey found that 4.9% of the 244 pulses that were run during the JET-C C27b He campaign and 15.3% of the 59 pulses during the JET-ILW C38 He experiment had significant opacity defined in terms of the length ($\geqslant 2$ s) over which the opacity was observed. Estimates of escape factors and optical depths have been determined for these pulses, with the optical depth reaching ~ 6 along the line-of-sight of the observing spectrometer in the most extreme case. Although this is expected to affect the distribution of radiation within the divertor, changes to the ionisation balance are expected to be minimal.

A comparison of the escape factor estimates with an infinite plane parallel slab model with uniform emission throughout the plasma volume and Gaussian spectral line profiles (Irons 1979) showed poor agreement. Consequently, an alternative model based on the present measurements has been derived using the C27b results, for which the opacity was found to be more severe due to its line-of-sight viewing the inner divertor. Although limited in range, the C38 escape factor estimates, for which the line-of-sight was different, also fitted the derived model suggesting that there was no strong sensitivity to differences in geometry. In contrast, the Lyman gamma escape factors tended to lie above the derived model. This brings into question the assumption that the curve describing the escape factor as a function of $k_0 D$ is the same for all lines. Since transport codes do not usually include photon transport for He II ions, any use of the listed pulses in transport simulations should be carried out with particular care.

The non-active start of research operations phase of ITER is now to use H and then D fuel, rather than He. Consequently, the increased path lengths in ITER are not expected to compensate for the lower concentrations of He, present only as ash resulting from the DT reactions. Given that He opacity in JET only affects extreme cases, it is not expected to be important in ITER. Nevertheless, the proposed method gives a simple procedure for checking for opacity.

The absorption in He I is higher ($\sim \times 2$) than found for He II. Even so the JET VUV He spectrum is dominated by He II with He I lines significantly weaker suggesting a lower density of the latter ionisation stage. This is expected to more than offset the higher absorption. The relationship between He II and He I observed in JET is expected to be found in ITER and other high temperature plasma machines.

Data availability statement

All data that support the findings of this study are included within the article (and any supplementary files).

Acknowledgment

We would like to thank Professor Greg Tallents for useful discussions.

This work has been carried out within the framework of the EUROfusion Consortium, funded by the European Union via the Euratom Research and Training Programme (Grant Agreement No. 101052200—EUROfusion) and from the RCUK Energy Programme [Grant Number EP/W006839/1]. The views and opinions expressed are however those of the authors only and do not necessarily reflect those of the European Union or the European Commission. Neither the European Union nor the European Commission can be held responsible for them.

ORCID iDs

K D Lawson 0000-0002-1251-6392
M Groth 0000-0001-7397-1586

References

Arnaud M and Rothenflug R 1985 *Astron. Astrophys. Suppl. Ser.* **60** 425
Behringer K 1998 Escape factors for line emission and population calculations *IPP Report* 10/11 (available at: https://hdl.handle.net/11858/00-001M-0000-0027-608E-E)
Behringer K and Fantz U 2000 *New J. Phys.* **2** 23

Chandra R *et al* 2024 *Nucl. Mater. Energy* **41** 101794
Holstein T 1947 *Phys. Rev.* **72** 1212
Huber A *et al* 2021 *Phys. Scr.* **96** 124046
Irons F E 1979 *J. Quant. Spectrosc. Radiat. Transfer* **22** 1
Lachin T 1998 *UCL PhD Thesis*
Lawson K D, Aggarwal K M, Coffey I H, Keenan F P and O'Mullane M G 2019 *J. Phys. B* **52** 045001
Lawson K D, Coffey I H, Groth M, Meigs A G, Menmuir S and Thomas B 2024 *Plasma Phys. Control. Fusion* **66** 115001
Lomanowski B, Groth M, Coffey I, Karhunen J, Maggi C F, Meigs A G, Menmuir S and O'Mullane M 2020 *Plasma Phys. Control. Fusion* **62** 065006
Lovegrove T *et al* 1995 *Proc. 22nd EPS Conf.* (*Bournemouth, UK*)
Maggi C F, Horton L D, Corrigan G, Jäckel H J, Loarte A, Monk R D, Simonini R, Stamp M and Taroni A 1999 *J. Nucl. Mater.* **266–269** 867
Pshenov A A *et al* 2023 *Nucl. Mater. Energy* **34** 101342
Reiter D, Wiesen S and Born M 2002 *Plasma Phys. Control. Fusion* **44** 1723
Scott H A and Mayle R W 1994 *Appl. Phys. B* **58** 35
Solano E R *et al* 2021 *Nucl. Fusion* **61** 124001
Tallents G J 2018 *An Introduction to the Atomic and Radiation Physics of Plasmas* (https://doi.org/10.1017/9781108303538)
Tallents G J 2019 *J. Appl. Phys.* **126** 083302
Wan A S, Dalhed H E, Scott H A, Post D E and Rognlien T D 1995 *J. Nucl. Mater.* **220–222** 1102
Wiesen S *et al* 2003 *Proc. 30th EPS Conf.* (*St. Petersburg, Russian Federation, ECA*) vol 27A pp P–3.194
Wiesen S 2005 Nichtlineare simulation von photonentransport in plasmen *PhD Thesis* Ruhr-Universität Bochum